Journal of Zhejiang University SCIENCE
ISSN 1009-3095
http://www.zju.edu.cn/jzus
E-mail: jzus@zju.edu.cn

Liver fibrosis identification based on ultrasound images captured under varied imaging protocols

CAO Gui-tao (曹桂涛)[1], SHI Peng-fei (施鹏飞)[†1], HU Bing (胡 兵)[2]

([1]*Institute of Image Processing and Pattern Recognition, Shanghai Jiao Tong University, Shanghai 200030, China*)

([2]*Department of Ultrasound in Medicine, Shanghai Sixth Hospital, Shanghai Jiao Tong University, Shanghai 200233, China*)

[†]E-mail: pfshi@sjtu.edu.cn

Received June 20, 2005; revision accepted Aug. 8, 2005

Abstract: Diagnostic ultrasound is a useful and noninvasive method in clinical medicine. Although due to its qualitative, subjective and experience-based nature, ultrasound image interpretation can be influenced by image conditions such as scanning frequency and machine settings. In this paper, a novel method is proposed to extract the liver features using the joint features of fractal dimension and the entropies of texture edge co-occurrence matrix based on ultrasound images, which is not sensitive to changes in emission frequency and gain. Then, Fisher linear classifier and support vector machine are employed to test a group of 99 in-vivo liver fibrosis images from 18 patients, as well as other 273 liver images from 18 normal human volunteers.

Key words: Liver fibrosis, Texture, Co-occurrence matrix, Fisher classifier, Support vector machine
doi:10.1631/jzus.2005.B1107 **Document code:** A **CLC number:** R445 ; TP391

INTRODUCTION

There are more than 20 million chronic hepatitis patients in China and 300 000 people die of liver related disease every year, which is widely recognized as an emerging public health crisis. Moreover, liver damage can cause higher than normal amounts of collagen fiber deposits in the extra-cellular spaces of the liver cells and cause the liver cells to lose blood and lead to liver fibrosis, which is a necessary stage to cirrhosis and a reversible consequence, so it is critical that the fibrosis status is detected and proper medication is administered in case of cirrhosis.

Biopsy is usually used for accurate identification of liver fibrosis, whose treatment with the use of diagnostic ultrasound has been a useful and noninvasive clinical method for over two decades. Several researchers diagnosed diffused liver diseases based on ultrasound images assisted by computerized tissue classification. Ogawa *et al*.(1998) introduced an artificial neural network for classifying diffuse liver disease such as chronic active hepatitis and liver cirrhosis. Feature parameters extracted from five ROIs (regions of interest) (32 pixels×32 pixels) in each image included variance of pixel values, coefficient of variation, annular Fourier power spectrum, longitudinal Fourier power spectrum of the same ROI, and variation of the mean of the five ROIs. Another two parameters, angular second moment and contrast, are calculated from gray level co-occurrence. Wu and Chen (1993) proposed a multi-resolution fractal feature based on wavelet decomposition and fractional Brownian motion model for detecting three sets of ultrasonic liver images: normal, hepatoma and cirrhosis. Mojsilović *et al*.(1998) described a new approach for texture characterization based on nonseparable quincunx wavelet decomposition and used energies of the transformed regions to characterize textures for discriminating three different tissue types of liver: normal, steatosis and cirrhosis. Kadah *et al*.(1996) confirmed the importance of the choice of classification techniques on the success classification rate for normal, fatty and cirrhotic liver. Feature extraction algorithms are proposed and further proc-

essed to obtain the minimum number parameters which present the most discriminating pattern space for classification are used to develop and compare both statistical and neural classifiers.

Yeh *et al*.(2003) used fresh postsurgical human liver samples to determine the grade of liver fibrosis from B-mode liver images. Image features derived from gray level co-occurrence and nonseparable wavelet transform were fed into a classifier known as support vector machine. For each specimen, 10 to 15 images from different scanning positions were acquired and only five subimages were selected. In each image, only one subimage of 64 pixels×64 pixels (approximately 1.5 cm×1.5 cm) was selected to ensure that the subimage only contained information from the specimen.

Due to its qualitative, subjective and experience-based nature, computerized ultrasound diagnosis has a lot of restricted applications in liver disease identification. The existing methods were all standardized for the scanner to ensure the fidelity of the tissue characterization procedures because the attenuation of ultrasonic waves depends mainly on the emission frequency, and machine settings such as time gain compensation (TGC), tissue enhanced imaging (TEI), focus, and gain (G), can change the overall images (Kadah *et al*., 1996).

Our experiments focus on applying a novel feature extraction method for discriminating the liver fibrosis from the in-vivo healthy ultrasound images captured in varied imaging conditions. This paper is organized as follows: after feature extraction approaches are proposed, the pattern classification techniques and experimental results follow. Finally, discussion and conclusions are presented.

FEATURES EXTRACTION

Two important characteristics of liver fibrosis are different granular sizes and uniformity of the liver parenchyma. A method is proposed in this study to interpret both the texture size and gray difference between liver lobule by fractal dimension and texture edge co-occurrence matrix, respectively.

Measurement of fractal dimension

'Fractal' is a term coined by Mandelbrot to describe the shape made of parts similar to the whole in some way (Mandelbrot, 1982). The property of self-similarity is a hallmark of the images known as fractals. As a bounded set A, in Euclidean n-space, is self-similar, if A is the union of N_r nonoverlapping copies of itself scaled down by a ratio, r, in all coordinates from the whole. The Hausdorff-Besocovitch dimension (fractal dimension) D_f of A can be derived from the relation:

$$D_f = \frac{\log(N_r)}{\log(1/r)} \tag{1}$$

While the definition of fractal dimension via self-similarity is straightforward, it is difficult to compute directly from the natural images because their self-similarity is statistical. Irregular fractals have many examples, such as discrete dot sets, coarse curve, two-dimensional graphics with many branches, coarse surface, and even three-dimensional dot sets or graphics. Fractal dimension provides a proper mathematical framework for studying these irregular and complex shapes that exist in nature. Hence, if the pixel intensity of ultrasound B-scan images is regarded as the height above a plane then the intensity surface can be viewed as a rugged surface. Among the present approaches estimating fractal dimension in an image, the differential box counting (DBC) method (Sarkar and Chaudhuri, 1994) that can cover a wide dynamic range and compute efficiently is adopted herein.

Consider an image of $M\times M$ pixels with $f(x, y)$ denoting the intensity, and (x, y) indicating the two-dimensional position. If the image is scaled down to $s\times s$ pixels (s is an integer, and $1<s\leq M/2$), scale ratio r becomes s/M. Then, $M\times M$ space can be partitioned into $s\times s$ grids with a column of $s\times s\times h$ boxes. Where, h is denoted by $[G/h]=[M/s]$, and G is the total number of gray-levels. Let the minimum and the maximum intensity of the image in the $(i, j)th$ grid both fall in the boxes k and l, as illustrated in Fig.1. Then

$$n_r(i, j)=l-k+1 \tag{2}$$

where, $n_r(i, j)$ is the contribution of N_r in the (i, j)th grid. Taking contributions from all grids, N_r is obtained for different r. So, the fractal dimension D_f can be estimated from the least-square linear fitting of

log(N_r) versus log(1/r).

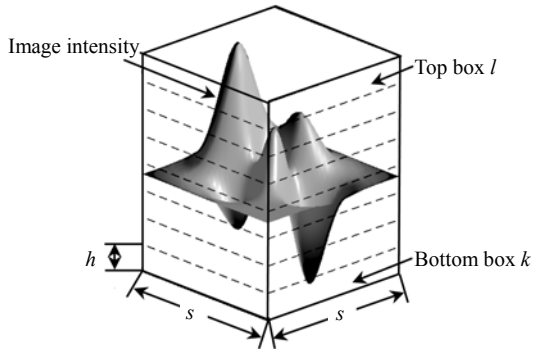

Fig.1 Determination of $n_r(i, j)$

Texture edge co-occurrence matrix

Texture is a feature used for comprehending the region of interest (ROI) and to classify those patterns, with their edges corresponding to the texture boundaries. According to Canny, a good edge detector should have the following three properties: (1) low probability of wrongly marking non-edge points and of failing to mark real edge points (i.e. good detection); (2) points marked as edges should be as close as possible to the center of true edges (i.e. good localization); and (3) one and only one response to a single edge point (single response). Canny edge detector (Canny, 1986) optimizes the trade-off between noise suppression and localization, and can be outlined as follows:

1. Smooth liver image with a Gaussian filter, with standard deviation σ=1 in our case;

2. Compute gradient magnitude and orientation using finite difference approximation;

3. Perform nonmaxima-suppression for each pixel along four directions: 0°, 45°, 90° and 135° orientations. Compare the gradient magnitude with its two neighbors and determine if it is a local maxima or not;

4. Extract edge by hysteresis thresholding. Set the gradient magnitude of the liver image to threshold with two different values T_1, T_2, and $T_1>T_2$. Mark pixels with values above threshold T_1 as texture edges. Mark pixels adjacent to the points (e.g. eight-connectivity) that have been marked as edge and with values above threshold T_2 as edges. Hysteresis thresholding can avoid losing faint edges and also ignore the noises.

After texture edge is detected, the texture edge co-occurrence matrix (TECM) can be derived from gray level co-occurrence matrix (GLCM) contributing to the perception of texture by identifying repeated spatial patterns (Haralick *et al*., 1973). This is done by computation of a number of co-occurrence matrices, which essentially measure the number of times a pair of pixels at some defined separation have a given pair of intensities. This configuration varies rapidly in fine textures, slowly in coarse textures. A co-occurrence matrix has a size equal to the number of gray levels in the image, and is computed for a given direction and a given distance.

The formal definition of gray-level co-occurrence matrix is as follows:

$$\begin{aligned} C_0(i,j) = \frac{1}{N}\text{cardinality}\{[(k,l),(m,n)] \in ROI : \\ |k-m|=\text{d}x,\ |l-n|=\text{d}y, \\ \text{sign}[(k-m)\cdot(l-n)]=\text{sign}(\text{d}x\cdot\text{d}y) \\ g(k,l)=i, g(m,n)=j\} \end{aligned} \tag{3}$$

where, $C_0(i, j)$ is the gray-level co-occurrence matrix entry at gray-level i and j, $g(i, j)$ is the gray-level of the pixel (i, j) in the ROI, N is the total number of pixels inside the ROI, and (dx, dy) is a prescribed neighborhood definition. In other words, the entry $C_0(i, j)$ describes how often the two gray-levels i and j are neighbors under the given neighborhood definition.

In texture edge images, $g(i, j)$ has two values, 0 and 1's, and GLCM becomes texture edge co-occurrence matrix (TECM). Now, the co-occurrence matrix becomes 2×2, and the entry has only four values $P_0(0, 0)$, $P_0(0, 1)$, $P_0(1, 0)$ and $P_0(1, 1)$. So, the entropy can be defined by Shannon's measure:

$$ENT = -\sum_{i,j\in\{0,1\}} P_0(i,j)\times\log P_0(i,j) \tag{4}$$

ENT will be largest when $P_0(i, j)$ are as uniform as possible, and smaller when they become distinct.

Joint features vector

In this study, a joint feature vector (J-FT) is denoted based on fractal dimension and the entropies of TECM as follows:

$$J\text{-}FT=[FD\ ENT] \tag{5}$$

where, FD is the fractal dimension, ENT the entropies of TECM calculated when (dx, dy) is (1, 0), (0, 1), (1, 1), (2, 0), (0, 2) and (2, 2) in this study, respectively. So, there are six entropies for training and test.

The ultrasound noise is a high-frequency signal, mostly affecting a single image point. So, Gaussian filter with 3×3 window and the standard deviation σ=0.5 is implemented to eliminate the noise influence before FD estimation.

PATTERN CLASSIFICATION ALGORITHMS

A set of parameters with reference to the classification results will be defined before the classifier is described (Kadah *et al*., 1996).

1. Sensitivity is the conditional probability of detecting the fibrosis while there is in fact fibrosis, which is defined as: sensitivity=1−false-negative rate. Where, false-negative rate is the probability that the discrimination result indicates a normal liver while the true diagnosis is liver fibrosis. This case should be avoided since it represents danger to the patient.

2. Specificity is the conditional probability of detecting a normal liver while the liver is indeed normal. It is defined as: specificity=1−false-positive rate. Where, false-positive rate is the probability that the classification result indicates liver fibrosis while the true diagnosis is indeed a normal liver.

3. Correct classification rate (CCR) is defined as $CCR=C/N$, where C is the number of correct classification cases and N is the total number of samples.

Fisher linear classifier

Fisher linear classifier (Bian and Zhang, 2000) plays an important role in mapping the data from multi to single dimension. There are k-dimensional samples $\boldsymbol{x}_n=\{x_1, x_2, \ldots, x_N\}$, where N_1 is the sample number belonging to ω_0 (normal), N_2 is the sample number belonging to ω_1 (fibrosis), and $N=N_1+N_2$ is the total number of samples. Each sample, $\boldsymbol{x}_i=[x_{i1}, x_{i2}, \ldots, x_{ik}]^{\mathrm{T}}$ (i=1, 2, …, N), is the ith sample formed by the extracted features. Estimate the within-class scatterness $\boldsymbol{S}$ of the training samples by:

$$\boldsymbol{S}=\sum_{x\in\omega_0}(x-m_1)(x-m_1)^{\mathrm{T}}+\sum_{x\in\omega_1}(x-m_2)(x-m_2)^{\mathrm{T}} \tag{6}$$

where, $m_1=\frac{1}{N_1}\sum_{x_i\in\omega_0}x_i$, $m_2=\frac{1}{N_2}\sum_{x_j\in\omega_1}x_j$.

Under the Gaussian assumption, best separation of two classes can be computed as:

$$\boldsymbol{W}^*=\boldsymbol{S}^{-1}(m_1-m_2) \tag{7}$$

Then, the k-dimensional samples can be mapped onto single-dimensional samples by:

$$y_n=\boldsymbol{W}^{*\mathrm{T}}\cdot x_n \tag{8}$$

If $\tilde{m}_1=\frac{1}{N_1}\sum_{y_i\in\omega_0}y_i$ and $\tilde{m}_2=\frac{1}{N_2}\sum_{y_j\in\omega_1}y_j$, the separating threshold Y_0 can be selected by:

$$Y_0=\frac{N_1\tilde{m}_1+N_2\tilde{m}_2}{N_1+N_2} \tag{9}$$

Subsequently, the Fisher classifier can be expressed by the following equation:

$$x_i\in\omega_0, \text{ if } y_i\geq Y_0, \text{ else } x_i\in\omega_1,\ i=1, 2, \ldots, N. \tag{10}$$

Support vector machine

Pattern recognition by support vector machine (SVM) may be stated as follows (Burges, 1998): Given a training set ($\boldsymbol{x}_i$, y_i) (where $\boldsymbol{x}_i$ comprises the input features, $y_i\in\{\pm1\}$ is the classification output, i=1, 2, …, N, and N is the number of samples). Optimal margin classification of linearly separable patterns is achieved by finding a hyperplane to separate the two classes {+1, −1} on either side of the hyperplane. The decision surface (the hyperplane) is as follows:

$$f(x)=\mathrm{sgn}\left(\sum_{i=1}^{N}y_i\alpha_i(\boldsymbol{x}_i\cdot\boldsymbol{x})+b\right) \tag{11}$$

where, the coefficients α_i and b can be determined by solving the large-scale quadratic programming problem:

$$\boldsymbol{W}(\alpha)=\sum_{i=1}^{N}\alpha_i-\frac{1}{2}\sum_{i,j=1}^{N}\alpha_i\alpha_j y_i y_j(\boldsymbol{x}_i\cdot\boldsymbol{x}_j) \quad (12)$$

which is subject to the constraints:

$$\sum_{i=1}^{l}\alpha_i y_i=0,\ 0\le\alpha_i\le C \ \text{ for } i=1, 2, \ldots, l \quad (13)$$

The parameter C corresponds to assigning a penalty to tune the tradeoff between minimizing empirical risk (e.g. training errors) and the complexity of the machine. Upon training, only a fraction of the α_i terms are nonzero. For those $\alpha_i S$ that are nonzero, the corresponding training examples must be nearest to the margins of the decision boundary. These examples are called support vectors.

In most real natural problems, the data are not linearly separable. In order to apply nonlinear transforms to the original data, multiplying all the terms in the feature vector with each other can create a higher dimensional vector. The basic idea is to map the data into another feature space $\boldsymbol{F}$ where the patterns are linearly separable with a high probability via a nonlinear map $\boldsymbol{\Phi}$: $\boldsymbol{R}^m\rightarrow\boldsymbol{F}$ and implement the above linear algorithm in $\boldsymbol{F}$. So, the solution has the form:

$$f(x)=\mathrm{sgn}\left(\sum_{i=1}^{N}y_i\alpha_i\boldsymbol{\Phi}(x_i)\boldsymbol{\Phi}(x)+b\right) \quad (14)$$

Accordingly, $\boldsymbol{F}$ usually must have very high dimensionality in order to be linearly separable. This can be resolved based on two observations: First, although some mappings have very high dimensionalities, their inner products can be easily computed, and second, all the $\boldsymbol{\Phi}$ mappings used in the SVM occur in the form of an inner product. So, all the occurrences of inner product resulting from two mappings can be replaced with the kernel function $\boldsymbol{K}$ defined as:

$$\boldsymbol{K}(x, y)=\boldsymbol{\Phi}(x)\cdot\boldsymbol{\Phi}(y) \quad (15)$$

Then, without considering the mapping $\boldsymbol{\Phi}$ explicitly, a nonlinear SVM can be constructed by selecting the proper kernel, and the decision function becomes:

$$f(x)=\mathrm{sgn}\left(\sum_{i=1}^{N}y_i\alpha_i\boldsymbol{K}(\boldsymbol{x}_i,\boldsymbol{x})+b\right) \quad (16)$$

Polynomial kernel function as one of the three common type kernel functions of SVM is used as:

$$\boldsymbol{K}(\boldsymbol{x}_i,\boldsymbol{x})=(\gamma\boldsymbol{x}_i^{\mathrm{T}}\cdot\boldsymbol{x}+c)^d,\ \gamma>0 \quad (17)$$

In this study, γ=1, c=1, and d=3.

EXPERIMENTS

Image acquisition

In this paper, all ultrasonic images are acquired from right livers through ESAOTE S.P.A. TECHNOS$^{\mathrm{MPX}}$ ultrasound scanner with different transducer frequency at Shanghai Sixth Hospital. The video signal transferred through an I-RGB50 frame grabber to an Ultrasound Report System Version 5.0.1 (Kingstar Winning Medical Technology Co. Ltd.) and digitized with 768 pixels×576 pixels and 24 b/pixel RGB. The resultant images are then sent to a personal computer for further processing. In the experiments, the color images are changed into intensity images with 256 gray-levels.

There are total of 372 in-vivo ultrasound images in the experiments included 99 fibrosis images from 18 patients and 273 healthy liver images from 18 normal human volunteers. Since this study addresses the issue of fibrosis identification in different imaging conditions, the emission frequency is 2.5, 3.5, 4.5, or 7 MHz, imaging depth is 130 mm, and gain (G) varies from 95 to 170. In addition, different focus lengths, different TGC and TEI (PEN (Penetration), GEN (General)) are also taken into consideration.

There are several reports that the location of the region of interest (ROI) within an image has dominant effect on the classification. The tissue samples in our experiments are chosen to be as homogenous as possible, avoiding major vessels and acoustic shadowing is important. As the ultrasound pattern exhibits different behavior along the path of the acoustic pulse, and as the lateral speckle pattern is strongly depth dependent, the selected region should be selected each time near the center of the image so that the distorting effects of the reverberations in the shallow

parts and the attenuation in the deep parts are avoided. One example of ROI selection is shown in Fig.2.

Fig.2 One example of ROI (64 pixels×64 pixels) selection from the liver ultrasound image

For comparison, subsamples from different images, including healthy and fibrosis liver parenchyma, their corresponding texture edge images and gray histograms are shown in Fig.3 and Fig.4, respectively. Among them, B:4.5 represents emission frequency of 4.5 MHZ, B:PEN represents Penetration (TEI), B:GEN represents General (TEI), G:105 represents gain (G) of 105, and so on. The texture edge is extracted by Canny operator and the image histogram shows the intensities distribution in the image, with horizontal axis representing the pixel value and the vertical axis representing the amount of the same pixel value. Fig.3 and Fig.4 show that the fibrosis livers have much sparser texture edge, and much wider intensity distribution than those of the healthy liver.

Experimental results

In this study, two subimages of 64 pixels×64 pixels were selected independently from each liver image. In patients with liver fibrosis, the final diagnosis was confirmed by liver biopsy. In this way, the whole data set contained 744 tissue subimages for training and classification.

Usually, the training set is used to derive the classifier parameters, while the test set is used to obtain the accuracy of classification. Wu and Chen (1993) and Oosterveld *et al*.(1993) used all the samples to evaluate the classifier based on the leave-one-out procedure (Nadler and Smith, 1993). Prior to proceeding with training process, the leave-one-out procedure is performed as follows: First, one of the samples is removed and the remaining samples are used to compute the classifier. Then, this classifier is applied to predict the class of the removed object. This process is repeatedly used on all possible unique sets of the other samples.

Mojsilović *et al*.(1998) divided the entire samples into two sets (A and B) taken from the same patients. In our experiments, both set A and set B had 372 samples. First, the training set was set A and the test set was set B. Then, the training and test set were alternated for cross-validation.

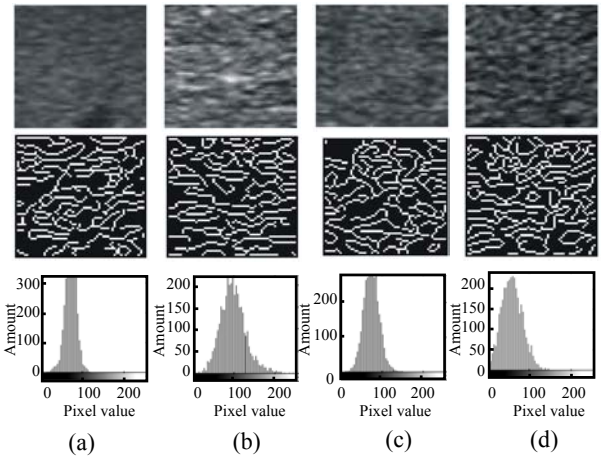

Fig.3 Healthy liver samples: first row, subsamples of 64 pixels×64 pixels; second row, texture edge images; third row, histograms: the amount of the same pixel value versus the pixel value (a) B:4.5, G:105; (b) B:GEN, G:155; (c) B:GEN, G:135; (d) B:GEN, G:115

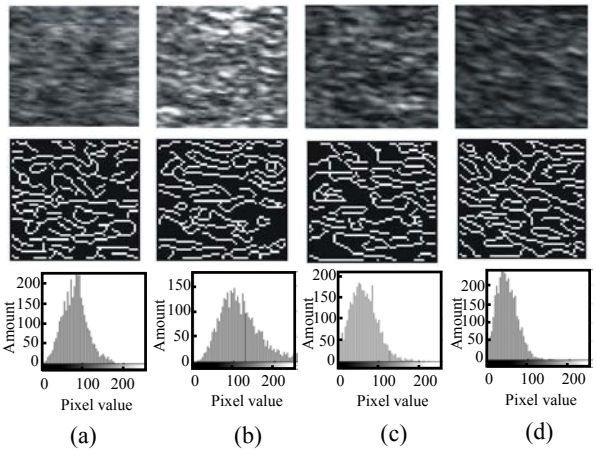

Fig.4 Liver fibrosis samples: First row, subsamples of 64 pixels×64 pixels; second row, texture edge images; third row, histograms: the amount of the same pixel value versus the pixel value (a) B:4.5, G:95; (b) B:GEN, G:150; (c) B:GEN, G:115; (d) B:GEN, G:100

Based on these three divisions of the entire sample set, experiments were performed both on FD and ENT using Fisher linear classifier, with the results in Table 1 showing obviously that the classification accuracy based on ENT is much more satisfactory than that based on FD with sensitivity of 94.9%, specificity of 79.9%, and CCR of 83.9%.

The classification results based on the joint features (J-FT) using Fisher classifier are shown in the columns 2, 4 and 6 of Table 2. Compared with the classification results based on ENT in Table 1, it can be found that J-FT improves the sensitivity from 94.9% to 95.9%, while increases the specificity from 79.95% to 81.3%, and CCR from 83.9% to 85.2%.

For comparison, we employ an SVM based on J-FT to evaluate the classification accuracy. The diagnostic results are given in columns 3, 5 and 7 in Table 2. It can be seen that there is no obviously different classification accuracy between the two classifiers.

DISCUSSION AND CONCLUSION

The ultrasound scanners in use can be adjusted to be optimal to different clinicians, so the scanning frequency and machine settings sometimes can greatly influence the liver images captured and impact further the automatic classification result. Table 3 shows an example of the calculated features of the images from the same healthy liver acquired at different gain (G) (where G is 95, 115, 125, 130, 135, 145, 150, and 170, respectively) when transducer frequency is 3.5 MHz. Where, FD is the fractal

Table 1 Diagnostic results (in percentage) of FD and ENT using Fisher classifier in terms of sensitivity, specificity and CCR

Data set	Training set: the entire sample*		Training set: set A; Test set: set B		Training set: set B; Test set: set A	
	FD	*ENT*	*FD*	*ENT*	*FD*	*ENT*
Sensitivity	65.7	94.9	62.6	93.9	65.7	94.9
Specificity	54.2	79.9	51.3	78.0	54.2	79.9
CCR	57.3	83.9	54.3	82.3	57.3	83.9

*Evaluated by Leave-one-out algorithm

Table 2 Diagnostic results (in percentage) of J-FT using Fisher classifier and SVM in terms of sensitivity, specificity and CCR

Data set	Training set: the entire sample*		Training set: set A; Test set: set B		Training set: set B; Test set: set A	
	Fisher	*SVM*	Fisher	*SVM*	Fisher	*SVM*
Sensitivity	94.9	93.9	94.9	93.9	95.9	94.9
Specificity	81.3	81.0	81.3	78.7	81.0	78.4
CCR	85.2	84.4	85.2	82.8	85.2	82.8

*Evaluated by Leave-one-out algorithm

Table 3 The calculated features of an example of healthy liver images acquired at different gain (G) (G is 95, 115, 125, 130, 135, 145, 150, and 170, respectively) when transducer frequency is 3.5 MHz

Features	*FD*	*ENT*					
Gain (G)		(0, 1)	(0, 2)	(1, 0)	(2, 0)	(1, 1)	(2, 2)
95	2.3462	0.9627	1.0160	1.0071	1.0160	1.0285	1.0323
115	2.2786	0.9718	1.0316	1.0374	1.0370	1.0539	1.0534
125	2.2957	0.9600	1.0111	1.0143	1.0145	1.0312	1.0300
130	2.2647	0.9775	1.0285	1.0266	1.0262	1.0428	1.0421
135	2.2810	1.0113	1.0572	1.0607	1.0563	1.0754	1.0734
145	2.3342	0.9976	1.0454	1.0408	1.0360	1.0623	1.0539
150	2.3079	0.9692	1.0118	1.0146	1.0125	1.0276	1.0267
170	2.2363	0.9662	1.0226	1.0195	1.0242	1.0568	1.0489

dimension estimated by differential box counting method, and ENT is the entropies when (dx, dy) is (0, 1), (0, 2), (1, 1), (2, 2), (1, 0), and (2, 0), respectively.

Table 3 clearly shows that with the gain changes, FD varies rapidly, while ENT varies slowly. That is why the classification accuracy based on ENT is much more satisfactory than that based on FD.

The fibrosis identification results using the joint features extracted from the fractal dimension and the entropies of the texture edge co-occurrence matrix are encouraging because both the size and distribution of lobular structure of the liver parenchyma are all taken into consideration. More work should be done to optimize this method for diagnosing liver fibrosis status and grade.

Furthermore, as each sample of 64 pixels×64 pixels has to be chosen carefully with the assistance of the physician, an automatic selection method for dataset should be developed.

References

Bian, Z.Q., Zhang, X.G., 2000. Pattern Recognition, 2nd Ed. Tsinghua University Press, Beijing, China, p.87-90 (in Chinese).

Burges, C.J.C., 1998. A tutorial on support vector machines for pattern recognition. *Data Mining Knowledge Discovery*, **2**:955-974.

Canny, J.F., 1986. A computational approach to edge detection. *IEEE Transactions on Pattern Analysis and Machine Intelligence*, **8**:679-698.

Haralick, R.M., Shanmugan, K., Dinstein, I., 1973. Texture feature for image classification. *IEEE Transactions on Systems, Man and Cybernetics*, **3**:610-621.

Kadah, Y.M., Farag, A.A., Zurada, J.M., Badawi, A.M., Youssef, A.M., 1996. Classification algorithms for quantitative tissue characterization of diffuse liver disease from ultrasound images. *IEEE Transactions on Medical Imaging*, **15**:466-478.

Mandelbrot, B.B., 1982. Fractal Geometry of Nature. Freman, San Francisco, CA.

Mojsilović, A., Popović, M., Marković, S., Krstić, M., 1998. Characterization of visually similar diffuse diseases from B-scan liver images using nonseparable wavelet transform. *IEEE Transactions on Medical Imaging*, **17**:541-549.

Nadler, M., Smith, E.P., 1993. Pattern Recognition Engineering. Wiley, New York.

Ogawa, K., Fukushima, M., Kubota, K., Hisa, N., 1998. Computer-aided diagnostic system for diffuse liver diseases with ultrasonography by neural network. *IEEE Transactions on Nuclear Science*, **45**:3069-3074.

Oosterveld, B.J., Thijssen, J.M., Hartman, P.C., Rosenbusch, G.J.E., 1993. Detection of diffuse liver disease by quantative echography: dependence on a priori choice of parameters. *Ultrasound in Medicine and Biology*, **19**(1):21-25.

Sarkar, N., Chaudhuri, B.B., 1994. An efficient differential box-counting approach to compute fractal dimension of image. *IEEE Transactions on Systems, Man and Cybernetics*, **24**:115-120.

Wu, C.M., Chen, Y.C., 1993. Multi-threshold dimension vector for texture analysis and its application to liver tissue classification. *Pattern Recognition*, **26**(1):137-144.

Yeh, W.C., Huang, S.W., Li, P.C., 2003. Liver fibrosis grade classification with B-mode ultrasound. *Ultrasound in Medicine and Biology*, **29**:1229-1235.